

Landslides (2024) 21:679–696
 DOI 10.1007/s10346-023-02178-5
 Received: 3 April 2023
 Accepted: 10 November 2023
 Published online: 22 December 2023
 The Author(s) 2023

Sabatino Cuomo  · Angela Di Perna · Mariagiovanna Moscarillo · Mario Martinelli



Possible remediation of impact-loading debris avalanches via fine long rooted grass: an experimental and material point method (MPM) analysis

Abstract Debris avalanches often originate along steep unsaturated slopes and have catastrophic consequences. However, their forecast and mitigation still pose relevant scientific challenges. This is also due to the variety of mechanisms observed near high sub-vertical bedrock outcrops, such as the impact loading of soil failed upslope the outcrop, the build-up of pore water pressures in the inception zone, and the bed entrainment along the landslide propagation path. At the University of Salerno, an experimental and numerical investigation campaign started some years ago to explore the feasibility of using long-root grass to mitigate or even inhibit the inception of debris avalanches. Previous laboratory results were achieved through two twin 2-m-long columns (one bare, one vegetated), where the change in soil retention curve and soil mechanical response was assessed. As follow-up, an experimental field setup was installed in 2020 first, and in an improved configuration in 2021. Here, three different species of long-root grass were grown. In situ soil suction and water content measurements were periodically collected in the vegetated and in the original soils. In both cases, soil specimens were also collected, and laboratory geotechnical tests were performed to individuate the changes in both the water retention and strength response. Increased values of soil suction and shear strength were outlined, despite some differences, for all the grown species compared to the original soil. Using these novel experimental data, advanced large-deformation stress–strain hydro-mechanically coupled analyses were recently performed through a material point method (MPM) approach. The original slope conditions were compared to various slope configurations engineered via long-root grass. The benefits and the open issues related to this novel green technology for landslide mitigation are discussed. Some insights are outlined for the possible reduction of the soil volumes mobilized inside the inception zone of debris avalanches.

Keywords Modelling · Landslide · Impact · Failure · Entrainment

Introduction

Modelling the flow-like landslides has been posing challenges to scientists for decades, mostly for their strongly different kinematic features during failure, post-failure, and propagation. This distinction in landslide stages is even oversimplified when heavy or prolonged rainfall causes an unsaturated shallow soil deposit to fail along a steep slope. In fact, after the formation of a first slip surface along the slope, cascading events may occur such as:

soil static liquefaction (if soils are loose or metastable), multiple retrogressive or progressive failures, loading of stable slope portions during the landslide propagation, the latter being also responsible of bed entrainment along the propagation path. Such mechanisms strictly interconnect the landslide stages. Soil deposit layering and engineering control works makes the landslide evolution even more complex.

Among the various types of flow-like landslides, debris avalanches (DA) were firstly classified by Hungr et al. (2001) as “very rapid to extremely rapid shallow flows of partially or fully saturated debris on a steep slope, without confinement in an established channel.” Cascini et al. (2013) observed that typical examples of DAs occur in colluvial soils of British Columbia (Hungr et al. 2008), torrent deposits of USA (Costa and Williams 1984), and decomposed granitic soils in Japan (Wang et al. 2003). Italy is also hugely affected by DAs, for instance, in debris deposits of Valtellina area (Northern Italy) as reported by Chen et al. (2006) and in the Vesuvian pyroclastic deposits in Southern Italy (Cascini et al. 2008a, b, Guadagno and Revellino 2005). The slopes affected are always very steep (even $> 40^\circ$), and failure occurs in cohesionless soil deposit often 1–2 m thick. In such contexts, creeping phenomena are not relevant. However, for all the abovementioned mechanisms, a small initial unstable volume (for instance, 100 to 1,000 m³) is later amplified by a factor of 10 to 50 in some cases, completely changing the magnitude of the event.

Two fundamental open issues are as follows: (i) how to reduce the amount of soil mobilised during the DA inception, possibly using eco-friendly solutions, (ii) how to assess the performance of those engineering control works.

The basic idea of this paper is to investigate the possibility to use long-root grass to reduce the volume of debris avalanches in the inception zone. Different types of grass and roots have been tested in the literature, with different scopes (Wu et al. 1979; Wu 2013; Ng et al. 2013a, b, 2016a, b). More recently, long-root grasses have been also tested in coarse-grained soils affected by shallow landslides (Capobianco 2018) and in fine-grained soils involved in slow-moving landslides (Tagarelli 2019).

The other indispensable ingredient is the possibility to assess the performance of this novel mitigation technique. Given the complex processes at hand, there is the need to use of a large-deformation stress–strain hydro-mechanical coupled approach. The latter must be capable to properly simulate either the cascading effects or the interaction of the landslide body with the engineered zones. A novel

mathematical approach named material point method (MPM) may contribute to solve some open questions. First introduced by Sulsky et al. (1994), MPM is particularly suitable for large deformations problems, firstly applied to slope stability by Cuomo et al. (2013), and to a number of different applications by Soga et al. (2016).

In this paper, the scientific literature about debris avalanches and soil-root interaction is briefly reviewed. Then, a theoretical framework is proposed for a new eco-friendly technique aimed to debris avalanche inception mitigation. The results of a laboratory and in-situ experimental campaign on artificially seeded soils are presented. Finally, a selected series of numerical simulations of debris avalanche inception in natural and engineered slopes are presented and discussed.

Literature review

Debris avalanches have been studied from different viewpoints. The combined mechanisms of (i) impact loading and (ii) propagation plus bed entrainment, with large increase in the unstable soil volume, have been evidenced in several geo-environmental contexts. Examples of torrent deposits mobilized due to undrained loading and build-up of excess pore water pressure have been described in Japan (Sassa et al., 1997; Wang et al. 2003). Similar mechanisms are reported by Cascini et al. (2008a) for shallow deposits of Vesuvian pyroclastic soils and formerly noted by Hutchinson and Bhandari (1971).

The “impact loading” mechanism was analyzed by Wang et al. (2002) and Sassa et al. (2003) through ring shear tests. The experiments demonstrated that the generation of excess pore pressure and soil contraction both contribute to large drop in soil shear resistance. However, a limitation of that time was to infer the slope-scale response from the laboratory-scale observations of soil behavior. On the other hand, first simplified limit equilibrium method analyses (at slope scale) of different loading scenarios, combined to differentiated stratigraphical settings and various soil pore water pressures at the impact, were also proposed (Cascini et al. 2008b). The numerical results highlighted that undrained loading and consequent build-up of pore water pressure can mobilize a landslide volume, whose amount depends on soil stratigraphy. The same authors also presented numerical finite element method (FEM) analyses of the undrained increase of pore water pressure due to dynamic loading. In these cases, an asymptotic trend of soil displacement over time was reproduced until the limit to lose the convergence of the numerical algorithm, which was casted only for small-strain problems at that time. Cascini et al. (2013) later performed hydro-mechanical coupled stress-strain analyses to demonstrate that this impact loading mechanism is self-propellent. Such indication was consistent with the laboratory results of ring shear tests developed by Japanese scholars (Sassa and co-workers).

The mechanism of “bed entrainment” occurs during the propagation stage, and it is the mobilization due to overload and shearing induced by the passage of the flow over a stable ground. Cuomo et al. (2014) explored the role of rheological features of the propagating mass combined to the geometry of the slope and to the features of the triggered volume. It was concluded that the lateral enlargement of a flowing mass along a slope is mostly regulated by bed shear resistance and slope steepness but soil thickness in the landslide source area also plays a role. Cuomo et al. (2016) extended the previous work to a series of past landslides, and they noticed

that the spatio-temporal pattern of the soil thickness eroded along a mountain catchment is complex and interconnected to the spatial distribution of slope morphology (e.g., channelized or not, etc.) and landslide dynamics features.

Both the mechanisms are relevant (Cuomo 2014), but each requires a specific approach in terms of governing equations to be incorporated in a model. For the impact loading, great accuracy is needed to describe the small-strain behavior of soils under dynamic conditions and the hydro-mechanical coupling between solid particles of soil and pore water. This is typically done via FEM (or similar tools) and using sophisticated soil constitutive models. Conversely, bed entrainment is typically accounted through propagation modelling approaches such as smooth particle hydrodynamics (SPH), or finite difference method (FDM), or discrete element method (DEM). These tools allow the simulation of large displacements of the soil from the triggering zone (and with runout distances even reaching some kilometers), but tremendously simplify the mechanical behavior of soil. This gap has been only recently bridged (Cuomo 2020). For instance, MPM and similar “particle” approaches allow tackling both the small-strain behavior under the dynamic impact and the later large displacements of the soil within a unique mathematical and numerical framework. A first contribution based on MPM was provided by Cuomo et al. (2021a), who quantified the extents of the zones where debris avalanches are initiated and then evolve.

Among the options to mitigate the dramatic effects of debris avalanches, the so-called active interventions aim at reducing the landslide volume inside the source areas. However, in steep areas, the feasible techniques are few due to the practical difficulties to reach the designated areas with standard construction machineries such as bulldozers, etc. Hence, one possible novel type of intervention could be based on the soil reinforcement by growing artificially seeded roots. The hydrological and mechanical effects of roots at different scales have been extensively reported in the literature (Boldrin et al. 2017; Leung et al. 2015, 2017; Ng et al. 2014, 2016a, b, c). Some roots mainly induce a change in soil suction and water content (Leung et al. 2015), while other types of roots are more capable to provide an additional shear strength (Stokes et al. 2009). More in general, the soil-root interaction comprises both hydrological and mechanical effects as evidenced by Capobianco et al. (2020) and Foresta et al. (2020). However, the use of artificially seeded roots to mitigate the magnitude of flow-like landslides has not yet explored up to now.

A new possible technique for the mitigation of debris avalanche inception

Theoretical framework

A new mitigation technique is proposed for the geo-environmental contexts characterized by steep slopes with shallow unsaturated soil deposits. These features are common, for instance, to the colluvium weathered covers in Brasil (Lacerda 2004) and Hong Kong (Fuchu et al. 1999), pyroclastic deposits in Central America (Capra et al. 2003) and New Zealand (Ekanayake and Philipps 2002), in situ weathered soils in Hong Kong (Take et al. 2004) and Japan (Wang et al. 2002).

In such contexts, unsaturated soil condition is important, and evapotranspiration can be highly emphasized by soil-root

interaction. In general, for the unsaturated soils we can refer to effective stress as formulated by Bishop (1954):

$$\sigma' = \sigma - p_a I + S_r(p_a - p_w)I \quad (1)$$

where σ' is the effective stress tensor, σ is total stress tensor, p_a is the air pore pressure, p_w is the pore water pressure, $s = p_a - p_w$ is the suction, S_r is the saturation degree, and I is the identity tensor of second order.

As vegetated soils are multiphase materials, it is worth noting that the roots induce changes in soil void ratio. Ng et al. (2016a, b, c) assume that part of the soil pore space is occupied by roots (Fig. 1) and express the void ratio as:

$$e = \frac{e_0 - R_v(1 + e_0)}{1 + R_v(1 + e_0)} \quad (2)$$

where e_0 is the void ratio of a bare soil (i.e., before root permeation), $R_v = V_r/V_{tot}$ is the root volume ratio (mm^3/mm^3), which defined as the total volume of roots (V_r) per unit volume of soil (V_{tot}).

A vegetated soil can be also described using the root area ratio (RAR), which is defined as the ratio of the sum of total root cross-section area (A_r) to the soil cross-section area (A_{tot}). The RAR can be converted in R_v , if a root is assumed with cylindrical shape (Ni et al. 2017) in a depth range Δh :

$$R_v = \frac{\sum V_r}{V_{tot}} = \frac{\sum (A_r \cdot \Delta h)}{A_{tot} \cdot \Delta h} = \frac{\sum A_r}{A_{tot}} = RAR \quad (3)$$

The soil water retention curve, namely the change in saturation degree due to a change of soil suction can be highly modified by roots. In fact, while roots are growing it is typical to observe some reduction in soil void ratio (e), hence the soil become denser. We may label this effect as a “density effect” (D). On the other hand, the inclusion of very fine roots (as we will see later on) implies a change in grain size distribution (GSD) because a finer material is added to the original soil. This could be called as “fine effect” (F), and it is independent on the state of the root, dry or wet, active or inactive depending on seasonal period and root growth stage. A representation of both the D and F effects is depicted in Fig. 2. The combination of the D and F effects is also interesting. Once the same amount of external water is provided to both natural and rooted soil, the volume of voids free for seepage is generally slightly lower than before. However, the saturation degree is almost the same. Hence, for the combined D and F effect, suction is increased in the vegetated soil (VEG) compared to the original non-vegetated soil (NV).

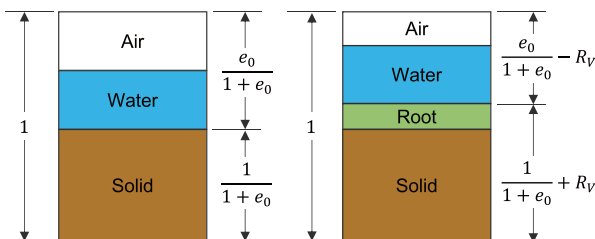


Fig. 1 Volumetric phase diagram of a bare (non-vegetated, NV) soil (on the left) and a vegetated (VEG) soil (on the right)

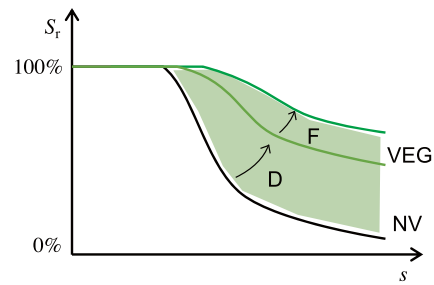


Fig. 2 Density (D) and fine (F) effects on saturation degree (S_r) and soil suction (s) due to vegetation roots (VEG) artificially grown in an unsaturated soil initially non-vegetated (NV)

The first key point of artificially seeded roots in a soil is the possible increase in soil suction, discussed so far. We may label it as “hydrological effect” (H) of artificial roots. Such increment has been widely documented in the literature, as previously discussed. In a context prone to landslide triggering, the increase in soil suction causes the increase in effective Bishop stress, and subsequently the increase in soil shear strength (Fig. 3).

Additional to those beneficial effects, there is the direct increase in soil shear strength due to the presence of long fine vertical roots, which provide additional tensile strength to the rooted soil. This is the “mechanical effect” (M) of artificial roots. A global measure of that is provided by the experimental determination of the shear strength envelope of the rooted soil, which always result in larger strength for a rooted (VEG) compared to a non-vegetated soil (NV). A representation of both the effects of the artificial roots on soil is given in Fig. 3. It is evident that the “hydrological effect” (H) improves somehow the initial soil condition before any failure occurs, while the “mechanical effect” (M) guarantees the increased strength of the rooted soil.

Practical implications

The landslide conceptual model proposed by Cascini et al. (2013) is adopted as guidance to discuss the debris avalanche mechanisms, later considered in the MPM hydro-mechanical simulations.

Two principal stages are considered for debris avalanche inception: (1) failure, when a soil mass becomes unstable even due to multiple triggering mechanisms; (2) avalanche formation,

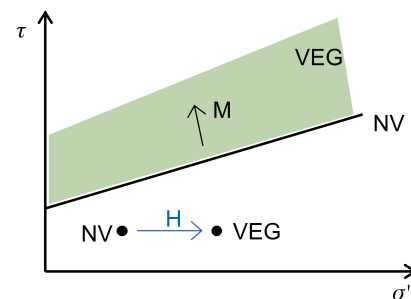


Fig. 3 Hydrological (H) and mechanical (M) effect of roots artificially grown in unsaturated soil

which is associated to the tremendous increase of the initial unstable volume.

The slope scheme includes an open slope interrupted by a sub-vertical bedrock outcrop which introduces both a cut slope and a free fall height for any soil eventually unstable at the edge (Fig. 4). Four distinct zones of the slope are individuated where one or more mechanisms take place. Inside zone 1, rainfall-induced slope failures occur at bedrock outcrops due to discontinuity of soil deposits. The zone 2 is the dynamic impact zone where the failed mass can mobilize the in-place soils. Inside zone 3, the failed mass thrusts the downslope soil and/or entrain further material from the ground surface. Zone 4 is controlled by interplay of propagation and bed entrainment. Hence, the landslide stages and the different zones (whose extent is unknown a priori) are intimately connected. Cascini et al. (2013) already observed that the zone 1 and zone 2 are relatively short (generally few tens of meters), while zone 3 and zone 4 may be much longer.

The initial value of in situ stress and its time evolution for significant points in the slope are here described referring to the stress invariants q and p' , and deviatoric strain ϵ_q which read as:

$$q = \frac{1}{\sqrt{2}} \sqrt{(\sigma'_{xx} - \sigma'_{yy})^2 + (\sigma'_{yy} - \sigma'_{zz})^2 + (\sigma'_{xx} - \sigma'_{zz})^2 + 6\sigma'_{xy}{}^2 + 6\sigma'_{yz}{}^2 + 6\sigma'_{zx}{}^2} \quad (4)$$

$$p' = \frac{\sigma'_{xx} + \sigma'_{yy} + \sigma'_{zz}}{3} \quad (5)$$

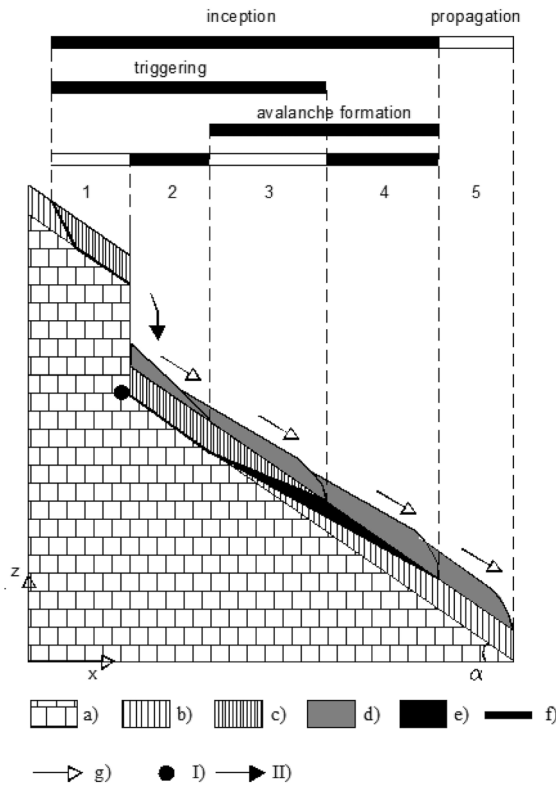
$$\epsilon_q = \frac{\sqrt{2}}{3} \sqrt{(\epsilon_{xx} - \epsilon_{yy})^2 + (\epsilon_{yy} - \epsilon_{zz})^2 + (\epsilon_{zz} - \epsilon_{xx})^2 + 6(\epsilon_{xy}{}^2 + \epsilon_{yz}{}^2 + \epsilon_{zx}{}^2)} \quad (6)$$

where p' is the mean effective stress, q is the deviatoric stress, ϵ_q is the deviatoric strain.

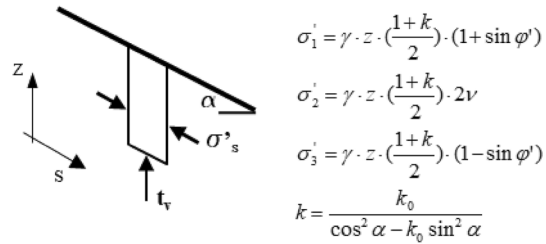
The initial in situ stresses are known for an infinite slope (Cascini et al. 2010), being related to earth pressure at rest (k_0), but they also depend much on slope steepness and soil suction. The steeper the slope the higher the stress ratio q/p' , given that p' is much related to soil thickness. However, soil suction makes p' to increase and the shear strength envelope to translate upwards in the q - p' plane (suction-related cohesion intercept, also named apparent cohesion).

The p' - q stress evolution is the outcome of the landslide mechanisms in the different zones. Inside zone 2 of the slope, the dynamic loading causes a large increase of q . The possible stress paths (Fig. 4) can be drained (case of region A of Fig. 4), undrained (region B), or intermediate depending on loading velocity and soil conductivity. On the hand, the rainfall-related processes such as infiltration from the slope ground surface, karst springs, runoff

a) Slope scheme



b) Mechanical scheme



c) Possible stress paths

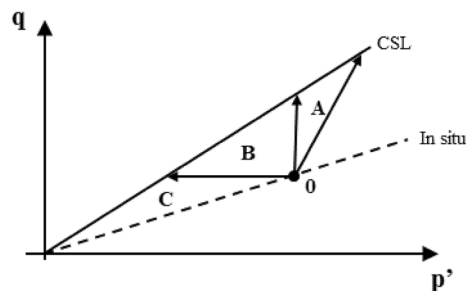


Fig. 4 Conceptual model for avalanche inception. **a** Slope scheme. Zones 1–2: triggering. Zone 3: thrust of failed material and/or soil entrainment. Zone 4: soil entrainment. Zone 5: propagation. (a) Bedrock, (b) stable soil deposit, (c) failed soil, (d) propagating failed mass, (e) entrained material, (f) boundary of debris avalanche, (g) propagation pattern. Triggering factors: (I) spring from bedrock, (II) impact loading. **b** Mechanical scheme: soil stress along an infinite slope. **c** Possible stress paths. drained impact (region A); undrained impact (region B), effect of a spring from bedrock (region C), static liquefaction (B and/or C), thrust of failed mass on stable soils (B or to be determined)

from bedrock outcrops cause p' to decrease (region C). More in general, the hydro-mechanical coupling between the solid skeleton and pore water plays a fundamental role. Soil static liquefaction can occur in loose metastable soils, and it is strongly related to the initial stress state in the q - p' plane (Fig. 4) and to the mechanical features of soils. In this case, the stress path moves in the region B and/or C of the q - p' plot of Fig. 4. The eventual generation of excess pore water pressure much depends on soil relative density and stiffness, the lower they are the higher is the excess pore water pressure generated upon impact loading. Generation of excess pore water pressure upon shearing (for increasing values of deviatoric strain ϵ_q) is also an important mechanism. Inside zone 3 of the slope, the thrust of an unstable mass upon stable soils cause an increase of deviatoric stresses and a stress path in the region B of q - p' plot of Fig. 4. Inside zone 3 and zone 4 of the slope, propagation-related entrainment from the ground surface causes more increase in q than in p' , and everything depends on the features of the flow, namely velocity, thickness, and rheology, not to mention the slope steepness, which is a fundamental factor as well.

An experimental campaign for artificially seeded rooted soils

Methods

The experimental campaign included in situ and laboratory investigations. The test site was selected inside the territory of Nocera Inferiore (Campania region, Southern Italy), which was affected by a dramatic debris avalanche in 2005, and it is similar to Sarno and other nearby cities hit by the 1998 catastrophic events (Cascini et al. 2008a, b). The test site was organized in 9 square plots, each $1\text{ m} \times 1\text{ m}$ large (Fig. 5a).

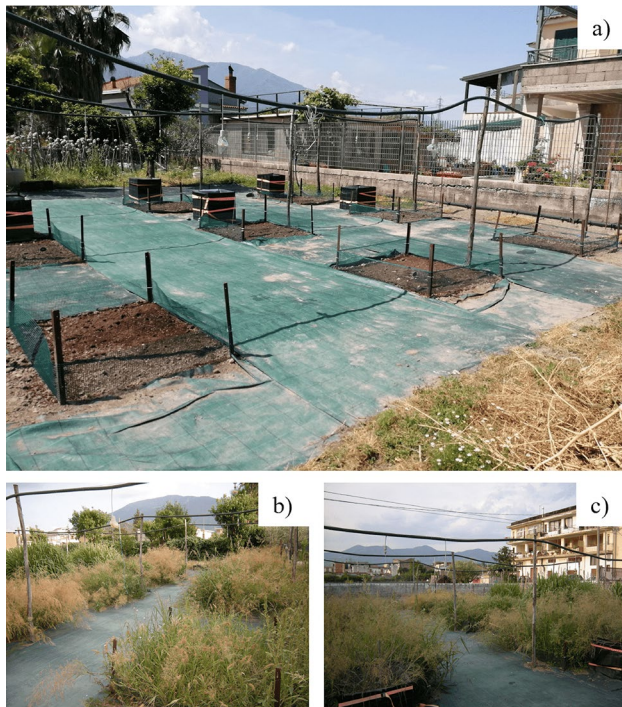


Fig. 5 Test site: **a** before seeding (Nocera Inferiore mounts are visible), **b** 3 months after seeding, **c** same as **b** with the Pizzo d'Alvano massif (affected by huge flow-landslides in 1998) as background

The tested soil is a pyroclastic non-plastic silty sand with median diameter equals to 0.425 mm , high value of porosity (0.55 – 0.58) and lightweight (11.04 – 12.82 kN/m^3). The granulometry and mechanical features of similar pyroclastic soils from nearby the study area is thoroughly reported in previous papers (Bilotta et al. 2005, 2008; Cuomo et al. 2015; Moscariello et al. 2021). Here, either hydraulic and shear strength features were investigated as described below.

For 6 months before the seeding (November 2020–May 2021), soil water content and suction were monitored. During this period, the soil was bare because the existing vegetation had been removed and neither native nor long-root grass were in place. The remotion of the original vegetation was necessary because the high density of the original vegetation did not allow adding other plants. The native grasses can be classified as Graminae and Asteraceae (Fратиanni et al. 2014; Strumia et al. 2020), with a plate root system and a tap root system (Switala 2016), with a maximum depth of 0.5 m .

The seeding was designed considering that hydroseeding with high germination rates is often used in the practice. The number of seeds per m^2 was calculated assuming a germination rate ranging from 85 to 95% , and a density investment of 1 seed each 1 cm^2 , being the specific weight of the seeds known for each of the species considered (VEG1, VEG2, VEG3). The used species can be referred as fine long-rooted perennial gramineae grass species, belonging to C3–C4 category with a high water consumptive demand and adaptive to xeric conditions (Ehleringer and Cerling 2002; Szarek and Ting 1975).

After seeding, soil matric suction was weekly measured at 0.2 m and 0.6 m while gravimetric water content (i.e., the wet soil mass minus the dry soil mass divided by the dry soil mass) was measured at the depth of 0.2 m . The suction was measured through a Quickdraw portable tensiometer, which provides the measurement within 15 – 30 s . The gravimetric water content was measured through a low-cost sensor which includes also sensors devoted to the measurement of soil temperature, light, Ph and nutrient. From the experimental results, the volumetric water content (i.e., the ratio of the volume of water to the unit volume of soil, the latter being dependent on soil porosity) was estimated considering three values of porosity, which correspond to the minimum, average and maximum values measured for the samples collected in the 9 plots over the time.

The field data of suction and water content were interpolated through the Van Genuchten equation (1980):

$$\theta = \theta_r + (\theta_s - \theta_r) \cdot \left[\frac{1}{1 + (\alpha s)^{n_{VG}}} \right]^m \quad (7)$$

where α , n , and $m = 1 - 1/n_{VG}$ are equation parameters, while θ is the volumetric water content, the subscripts r and s indicate the residual and the saturated values of θ .

Cumulated daily rainfall and the daily minimum and maximum atmospheric temperature data were acquired from a weather station of Campania Region located close to the experimental field setup. These data were used to define the boundary conditions in the test site. The temperature data were adopted to estimate the potential evapotranspiration (ET_0) through the Hargreaves (1975) equation modified by Mendicino and Senatore (2013), as follows:

$$ET_0 = C \cdot R_c(T + 17.8) \cdot \sqrt{\Delta T} \quad (8)$$

where C is the empirical Hargreaves coefficient, equal to 0.0023; R_e is the water equivalent of extraterrestrial radiation (mm/d), which depends on the inverse relative distance Earth-Sun, the sunset hour angle, and the solar declination; T is the mean daily temperature ($^{\circ}\text{C}$); ΔT daily temperature range ($^{\circ}\text{C}$).

The expected evapotranspiration (ET) was estimated multiplying ET_0 times the crop coefficient (k_c), which incorporates the features and the growth of the grass species. The crop coefficient also considers the dependence of ET on the leaf area index, LAI (Monteith 1965). The LAI is a dimensionless quantity that characterizes the plant canopies and it is estimated as the ratio between the leaf area and the ground area. In this paper, k_c was assumed equals 0.4 at initial stage, when the LAI exhibited values lower than 10%. The maximum k_c value is 1.3, here assumed for those months with the maximum annual growth of grasses and with the LAI approaching 100%. During the growth or during the dormancy period, the crop coefficient varies linearly between 0.4 and 1.3. Hereafter, the evapotranspiration is only considered as a component of the hydrological rainfall-evapotranspiration balance to check the reliability of the water content measurements.

The growth of the grasses was monitored monthly also collecting samples of the leaves of the three species and measuring their length, as done by Capobianco et al. (2020). In that study, the root length and leaf length were well correlated to the age of the grasses.

More than 40 specimens of the vegetated (VEG) and non-vegetated (NV) soil were collected manually up the depth of 0.30 m. The laboratory testing program was designed to investigate the changes in soil shear strength induced by the long fine roots of the three species (VEG1, VEG2, and VEG3) here investigated.

Direct shear tests on saturated and unsaturated soils were performed at constant water content or at constant suction. The shear strength of the vegetated and non-vegetated soils was described using the failure criterion proposed by Fredlund and Rahardjo (1993):

$$\tau_f = c' + (\sigma_v - u_a) \tan \varphi' + S_r \cdot s \cdot \tan \varphi' \quad (9)$$

where c' is the effective cohesion, $(\sigma_v - u_a)$ is the net vertical stress, φ' is the effective friction angle, with the saturation degree also equal related to soil porosity as follows $S_r = \theta/n = \theta \cdot (1+e)/e$.

This equation was already used to interpret the shear strength of the bare pyroclastic soils by Cuomo et al. (2017) and Moscariello et al. (2020), and it was also used here for the cases with vegetation,

being both the saturation degree and the void ratio dependent on the presence of roots. Moreover, the root reinforcement was conveniently expressed through an increased intercept cohesion (c_r) as proposed by Wu et al. (1979) in a semi-empirical expression later modified by Preti and Schwarz (2006), as follows:

$$c_r = 0.4 \cdot (\sin \xi + \cos \xi \tan \varphi') \cdot T_r \cdot RAR \quad (10)$$

where ξ is the angle of shear distortion in the shear zone at root breakage; T_r is the average root tensile strength, $\sin \xi + \cos \xi \tan \varphi' = 1.2$, and it is assumed that all the roots break simultaneously.

Experimental results

The long-root grasses were planted in the late spring (21 May 2021), and after 15 days, the first leaves appeared. The height of foliage acquired during a year of observation is reported in Fig. 6a and compared to those of Capobianco et al. (2020). In field test site, the growth rate was higher than that observed in the twin columns (0.084 m/month), and after some months at a constant growth rate, the height of foliage remained constant. Later, the grasses passed to a dormancy stage. The highest growth rate was for the species VEG2 (0.73 m/month in the first 50 days), while the lowest growth for the species VEG1 (0.11 m/month in the first 50 days). The maximum height of foliage was exhibited by species VEG2, while even the species VEG1 reached a larger height than in Capobianco et al (2020).

The root diameters were also measured and plotted in Fig. 6b. The data are summarized through box plots, where the central mark indicates the median value, and the bottom and the top edges of the box indicate the 25th and 75th percentiles, respectively. Independent on the species, the median diameter was about 0.5 mm, consistent with Foresta et al. (2020). The species VEG2 exhibited the maximum median diameter of 0.50 mm, and the largest range of variation between the 25th and 75th percentiles (Fig. 7).

The three perennial gramineae grass species developed with a different root morphology (Fig. 8). The species VEG1 (Fig. 8a) has vertical, oblique, and deep tap roots; the roots are thin and originate from the stem of the grass; the main and the secondary roots have comparable diameters. The species VEG2 (Fig. 8b) has a root morphology similar to VEG1, but the roots are coated with jelly-like substance; moreover, the main and the secondary roots have slightly different diameters. The species VEG3 (Fig. 8c)

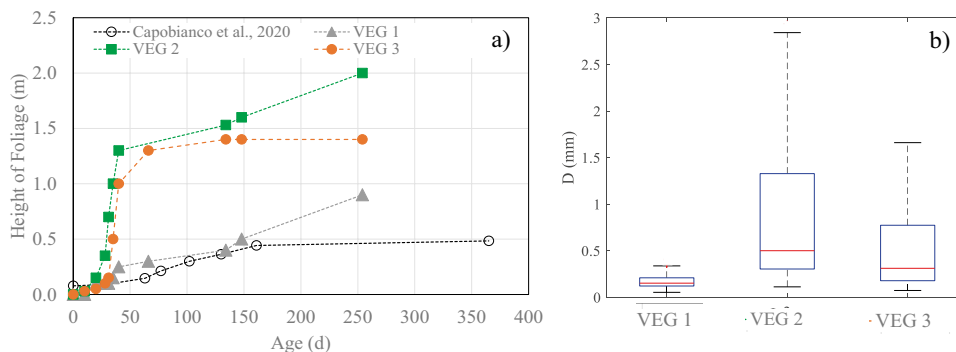


Fig. 6 a Growth rate for the three species. b Summary statistics on root measured diameter. The total number of measurements is 905, i.e., VEG1 ($n=244$), VEG2 ($n=249$), VEG3 ($n=412$)



Fig. 7 Leaves of **a** species VEG1, **b** species VEG2, and **c** species VEG3 collected in October–November 2021

exhibits a tap system with one large central fibrous root and finer lateral roots. For all the species, the rooting depth reached about 1 m in 1 year.

The experimental results of the in situ investigation are shown in Fig. 9a–d in terms of volumetric water content and matric suction, and in relation to evapotranspiration (*ET*). The latter increased in the summer season in which the *LAI* approaches to its highest value and the leaf reached their annual maximum length. The *ET* induces changes in suction measurements at low dept. (0.20 m). During the winter season, the *ET* is low, even if the *LAI* is high, and this is due to the dormancy period of the grasses.

The water content and the suction were always affected by rainfall and evapotranspiration seasonal trends (Fig. 9b). The water content in the vegetated soils was always lower than in the non-vegetated soils. Among the vegetation species, VEG1 exhibited the highest value of water content. Higher suction was also found in the vegetated ones compared to the non-vegetated soils. In terms of suction at 0.2 m, large differences between the vegetated and the non-vegetated soil started few days after the seeding (Fig. 9c). At 0.6 m, the difference in suction for the non-vegetated and vegetated soils appeared after 9 months (Fig. 9d). This is consistent with the growth of long-root grass species, which reached 1 m of depth in about 1 year.

The SWRC obtained interpolating the field data at 0.2 m are plotted in Fig. 10, and three values of void ratio adopted and the van Genuchten parameters for each kind of soil are summarized in Table 1. The presence of roots implied (i) a reduction of porosity and saturated water content, (ii) an increase of air entry value, and (iii) a slight reduction in residual water content. These observations are consistent with Leung et al. (2015), who asserted that the most preponderant effect of roots is on the SWRCs.

The shear strength parameters were estimated through laboratory tests (direct shear tests). It was assumed for the interpretation of the experimental results that the roots can be consider normal to the shear band and the assumption was supported by some formerly investigation (Fan and Su 2008; Mickovski et al. 2009; Yildiz et al. 2018. Moreover, it was as negligible the effect of root configuration on the interpretation of the results of laboratory tests. Under these assumptions, the shear strength was found as increased by root-soil interaction, but each type of grass affected the failure criterion in a different way (Fig. 11). While the intercept cohesion of the non-vegetated soil was very low (6.44 kPa), the maximum cohesion was exhibited by the grass species VEG2 (with $c' = 42.43$ kPa), but also the species VEG1 and VEG3 exhibited a significant increase of cohesion up to reach 20 kPa and 29 kPa,

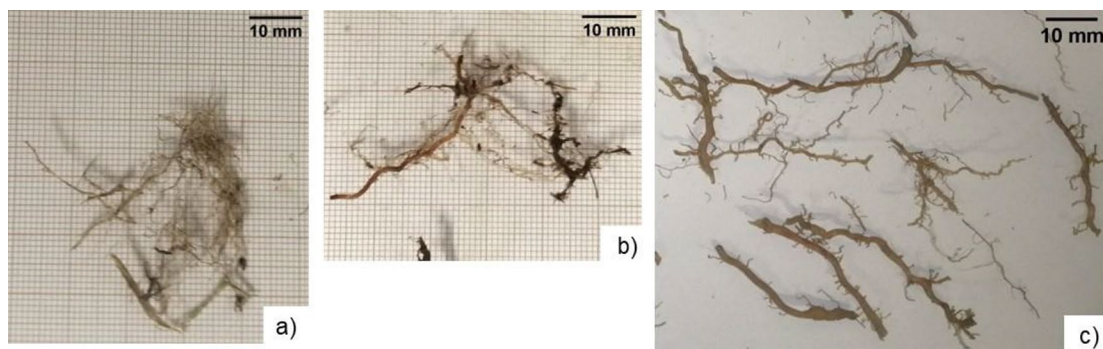


Fig. 8 Root morphologies of the three perennial gramineae grass species: **a** VEG1, **b** VEG2, **c** VEG3

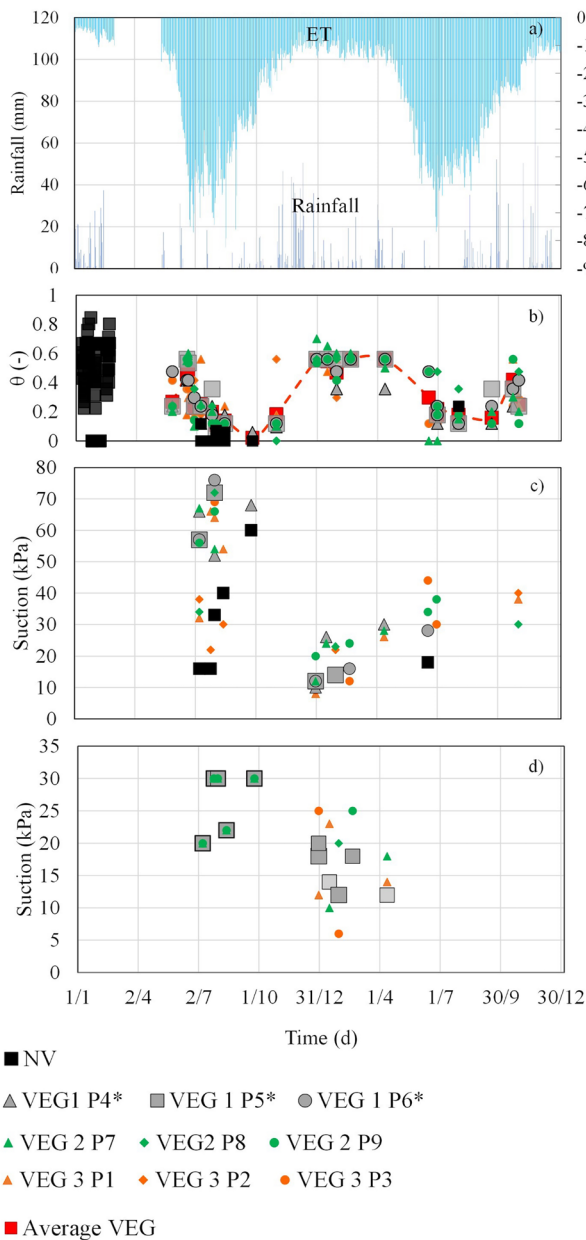


Fig. 9 a Rainfall and estimation of evapotranspiration for vegetated soil; b volumetric water content; c suction at 0.20 m of depth; d suction at 0.60 m. Gray corresponds to VEG1; green corresponds to VEG2; orange corresponds to VEG3

respectively (Table 2). Due to the intrusion of these very fine roots, the soil friction angle of vegetated soils is slightly lower than in the original non-vegetated soil (Table 2). The latter is surely a drawback, but in the practical applications where the in situ stresses are low (e.g., lower than 100 kPa), the shear resistance of the vegetated soils is always larger than that of non-vegetated soil, for all the three species here investigated (Fig. 11). In the figure, R^2 indicates the coefficient of determination (that is a well-known statistical measure) to emphasize that the data of VEG1 and VEG2 are less scattered than VEG3.

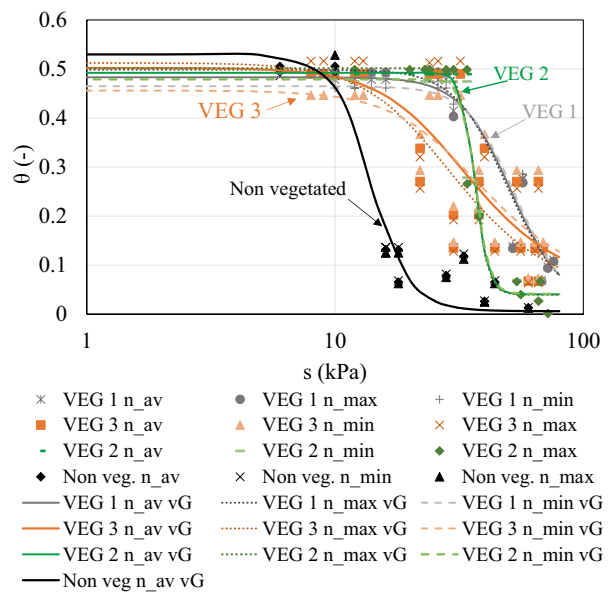


Fig. 10 Soil water retention curves of non-vegetated soil (NV) and vegetated soils (VEG1, VEG2, and VEG3). In the legend, the term “n” means porosity, while “av,” “min,” and “max” means that the volumetric water content was estimated considering the average porosity, minimum porosity, and maximum porosity, respectively. The label “vG” is referred to the interpolation curve of experimental data (markers) obtained using the van Genuchten equation

Large-deformation modelling of debris avalanche inception

MPM analyses: computational schemes and input data

The problem of the rapid propagation of a saturated mass flowing above a still unsaturated soil is very complex. To the knowledge of the authors, the first attempt has been proposed very recently (Cuomo et al. 2021a). From that pioneering yet simplified study, further research has allowed to incorporate a robust dataset for the (i) natural slope and (ii) engineered slope cases. The approach here used is hydro-mechanical coupled, meaning that a variation of pore water pressure induces an effective stress modification and a relative deformation. But also, the opposite situation is account for, so that for instance a reduction in soil volume (volumetric strain) induces a pore water pressure increase, and vice versa. In addition, the formulation in terms of Bishop effective stress is general to consider both saturated and unsaturated zones, where the pore water pressures are positive and negative, respectively. The flowing material is rapidly sheared and likely dilates while it is largely displaced downwards. On the other hand, the soil along slope where the flow propagates over is sheared and compressed by the moving flow. Such complex hydro-mechanical large displacement processes require the use of powerful tools such as MPM.

MPM is an enhancement of FEM, where the continuum body is schematized by a set of Lagrangian points, called material points (MPs), which move through a background computational mesh. Large deformations are modelled by these MPs, which carry all the physical properties of the continuum such as stress, strain, density, momentum, material parameters, and other state parameters,

Table 1 Parameters of van Genuchten equation (Eq. 8) for non-vegetated soil (NV) and vegetated soils (VEG1, VEG2, and VEG3)

	NV	VEG1		VEG2			VEG3			
	Aver.	Aver.	Max	Min	Aver.	Max	Min	Aver.	Max	MIN
n (-)	0.51	0.48	0.49	0.46	0.49	0.50	0.47	0.49	0.52	0.45
θ_s (-)	0.51	0.48	0.49	0.46	0.49	0.50	0.47	0.49	0.52	0.45
θ_r (-)	0.06	0.00	0.00	0.00	0.04	0.04	0.04	0.05	0.03	0.04
α (1/kPa)	0.08	0.02	0.02	0.02	0.03	0.03	0.03	0.04	0.04	0.03
n_{VG} (-)	10.22	4.35	4.22	4.59	16.00	16.15	15.62	2.71	2.65	2.64
a.e.v. (kPa)	13.3	47.9	46.1	50.3	27.3	23.7	30.9	36.4	36.2	36.6

n porosity, θ_s saturated volumetric water content, θ_r residual volumetric water content, n_{VG} and α fitting parameters of van Genuchten equation, a.e.v. air entry value

whereas the background mesh is used to solve the governing equations without storing any permanent information.

Unsaturated soils involved in slope stability problems can be conveniently modelled through the *two-phase single-point* formulation (Jassim et al. 2013; Ceccato et al. 2018; Cuomo et al. 2021b), which uses only one set of MPs for modelling the two phases (solid and liquid), whose accelerations are the primary unknowns. It is here assumed: (i) incompressible solid grains, isothermal condition, and no mass exchange between solid and liquid, as not relevant for most of the landslides; (ii) smooth spatial distribution of porosity and degree of saturation in the soil (Martinelli et al. 2021).

In such coupled hydro-mechanical approach, the dynamic motion of a partially saturated soil is described by the system of two momentum balance equations, using separate velocity fields for solid and liquid phase. The interested readers can find more information about this formulation in Cuomo et al. (2021b) and Yerro et al. (2022). The concepts of Bishop (1954) effective stress and Van Genuchten equation (1980) were used for modelling the response of unsaturated soils, consistently with the approach used to interpret

the experimental results. On the other hand, the dependency of hydraulic conductivity with suction was not considered, therefore the saturated value is used for all the soils. This is a safe assumption related to the fact that the initial in situ soil suction values are very low: 0 kPa for material 1 where the slope instability is triggered, 5 kPa for material 2 where the debris avalanche evolves.

Simplified yet realistic schemes were considered to test the efficacy of the remediation via long-root grass under different conditions. The reference scheme is represented in Fig. 12, in which the unstable mass is in a fully saturated condition while the soil on the slope downstream is stable in unsaturated condition due to the presence of soil suction s_o . The unstable soil (about 20 m³/m in volume) with uniform depth d_i , length B_i , and slope i_i falls from a height H and crashes on the stable slope which has depth H_s , length B_s and overall inclination i_s . A remediation measure via long-root grass is even modelled with depth d_v , length B_v , and initial suction $s_{o,v} > s_o$. The values of all the geometric features were chosen based on field evidence (Cascini et al. 2013) and are reported in Table 3.

In particular, “Geo 0” refers to the case in which the remediation is not installed, while going from “Geo 1” to “Geo 3” the vegetated zone is progressively reduced to analyse the influence of the grass extension.

In this paper, we do not develop slope stability analysis of the first moving mass, and we do not consider the effect of rainfall, with related soil infiltration and pore water pressure changes with eventual water table fluctuations, as previously done by Cascini et al. (2010) among others. In this study, we consider that in the upper zone, the soil is in an unstable condition from the beginning (linear distribution of pore water pressure, that is a very severe condition for such a case) and we simulate two fundamental yet challenging

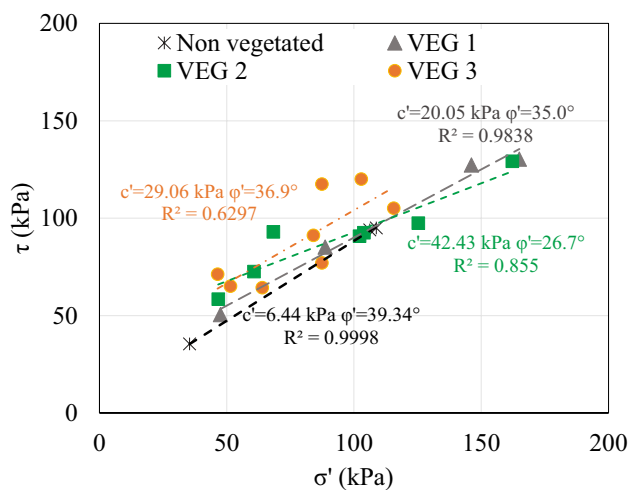


Fig. 11 Shear failure envelopes of the non-vegetated soil (NV) and the vegetated soils (VEG1, VEG2, VEG3), with R^2 indicating the coefficient of determination

Table 2 Shear strength envelopes (Eq. 9) for non-vegetated and vegetated soils

	NV	VEG1	VEG2	VEG3
c' (kPa)	6.44	20.05	42.43	29.06
ϕ' (°)	39.34	35.01	26.73	36.88
R^2 (-)	0.99	0.98	0.85	0.63

c' effective cohesion, ϕ' effective friction angle, R^2 coefficient of determination

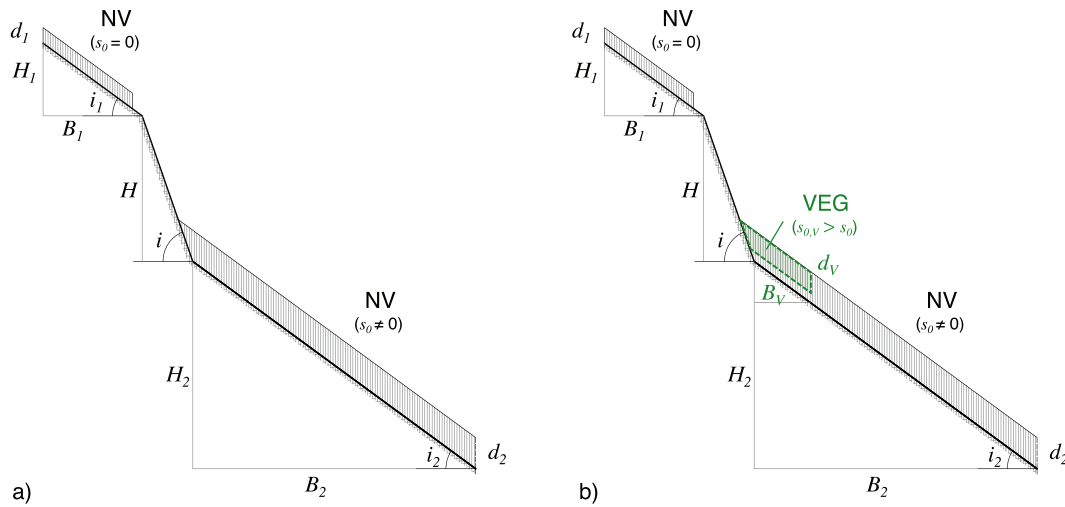


Fig. 12 Reference scheme for numerical analyses: **a** natural slope (NV); **b** slope engineered with long-root grass (VEG)

issues: (i) how this mass propagates downwards a steep slope, (ii) how this mass interacts with the lower unsaturated soil (where pore water pressure are still negative). The seasonal variations of suction are responsible for the type of slope instability phenomena and for the attained of slope failure (Cascini et al. 2014). In this paper, the role of suction (negative pore water pressure) in the whole process is considered in the analysis, which however refers to the challenging topic of how a small slide can provoke a much larger debris avalanche. This dynamic process is very fast, lasting few seconds, and the variation of pore water pressures (either negative or positive) are computed thanks to the hydro-mechanical coupled approach used here.

The mechanical properties of the non-vegetated soil (NV), such as shear strength, stiffness, saturated permeability, and unit weight (Table 4), are the typical values of the coarser superficial ashy soils (silty sands), having been widely investigated by Bilotta et al. (2005). For the vegetated soils, these properties are derived from the mean values of the experimental results for all the grass species (Table 1). On the other hand, the saturated hydraulic conductivity k_{sat} and water bulk modulus K_L are typical of fine sands.

The numerical mesh is made of 2294 quadrangular elements with size between 0.4 and 3 m (Fig. 13), and it is the same for all the 10 simulations reported in Table 5. The contact with the bedrock below (schematized as a rigid material) is handled with a frictional

contact algorithm. An improved contact algorithm was used, proposed by Martinelli and Galavi (2022), where the velocity of the liquid phase is corrected to prevent both inflow and outflow.

The standard linear 4-noded quadrilateral elements suffer from volumetric locking. To mitigate this problem, the B-bar method is used (Hughes 2012) in the proposed MPM formulation. Gauss integration is adopted to mitigate stress oscillation, and it is extended to 4-node quadrilateral elements. The reader can refer to Martinelli and Galavi (2022) for further details.

Based on previous experimental results (triaxial compression drained tests) reported by Foresta et al. (2020), it is inferred that Young’s modulus (E) of the vegetated soils can be increased up 3–5 times, depending on the confining stress; the lower the confining stress, the more the stiffness is increased. In the numerical analyses, the original stiffness and a doubled value increase were both considered for the vegetated soils.

Numerical results

The numerical results aimed to assess the feasibility of fine long-root grass for slope remediation, analyzing the time–space evolution of some quantities, such as stress, strain, pore pressure, and

Table 3 Geometric features of the simulation cases and installation mode

ID	Upper slope				Outcrop		Lower slope				Vegetation at lower slope	
	H_1 (m)	d_1 (m)	B_1 (m)	i_1 (°)	H (m)	i (°)	H_2 (m)	d_2 (m)	B_2 (m)	i_2 (°)	d_v (m)	B_v (m)
Geo 0	10	1.50	14	35	40	70	73	3	105	35	-	-
Geo 1	10	1.50	14	35	40	70	73	3	105	35	2	105
Geo 2	10	1.50	14	35	40	70	73	3	105	35	2	50
Geo 3	10	1.50	14	35	40	70	73	3	105	35	2	15

d_1 upper slope uniform depth, B_1 upper slope length, i_1 upper slope inclination, H outcrop height, i outcrop inclination, d_2 lower slope depth, B_2 lower slope length, i_2 lower slope inclination, H_v vegetated soil depth, B_v vegetated soil length

Table 4 Material properties used in the numerical analyses

Soil	ρ_{sat} (kg/m ³)	n (-)	E (MPa)	ν (-)	c' (kPa)	ϕ' (°)	ψ' (°)	σ_t (kPa)	k_{sat} (m/s)	K_L (MPa)	a.e. (kPa)	n_{vG} (-)
NV	1353	0.53	5	0.29	6.4	39.3	0	0	10^{-4}	50	13.3	10.22
VEG1	1390	0.48	5–10	0.29	42.4	26.7	0	0	10^{-4}	50	47.9	4.35
VEG2	1383	0.49	5–10	0.29	20.0	35.0	0	0	10^{-4}	50	36.4	15.99
VEG3	1375	0.50	5–10	0.29	29.0	36.9	0	0	10^{-4}	50	27.3	2.71

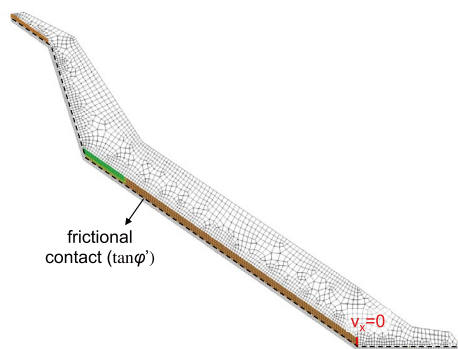
ρ_{sat} saturated soil density, n soil porosity, E Young's modulus, ν Poisson ratio, c' intercept cohesion, ϕ' effective friction angle, ψ' dilatancy angle, σ_t tensile strength, k_{sat} hydraulic conductivity, K_L water bulk modulus, a.e.v. air entry value, n_{vG} van Genuchten parameter

displacements, for all the abovementioned cases. Firstly, the spatial distribution for some relevant time lapses is considered. The case of natural slope without remediation (Fig. 14) is always used to compare the efficacy of the proposed solutions. For such situation (case 0), the impacting mass suddenly leads the below material to instability, due to the increase of pore-water pressure at impact. In fact, from the initial condition with suction $s_o = 5$ kPa, the liquid pressure increases up to 60 kPa ($t = 6$ s). Then, the blue zone with high pore-water pressure propagates downwards, leading to the liquefaction of the material, reaching very deformations during the simulation ($\epsilon_d > 1$). The debris avalanche develops in few seconds (about 20 s).

The efficacy of the proposed remediation measures via long-root grass is investigated in the following. The results collected for installation mode with $B_v = 15$ m (i.e., 1_3, 2_3, and 3_3 in Table 5) are reported for all the vegetation species: 1 (Fig. 15), 2 (Fig. 16), and 3 (Fig. 17).

Comparing the three remediation options (Figs. 15, 16, and 17), it is immediate to understand that the proposed solutions are effective. This is principally due to the increased strength of the vegetated soils, in terms of higher initial suction ($s_{o,v} > s_o$) and better mechanical properties. It can be seen for example that at impact the generation of both deviatoric strain and excess pore-water pressure is limited to a smaller zone than for case 0, avoiding the propagation of the high pore water pressure downwards.

Even the maximum values of pore-water pressure at impact ($t = 6$ s) are lower for the case with remediation than for case 0, as

**Fig. 13** Example of computational mesh used in the numerical analyses (installation mode: Geo 3)

they are halved. The deviatoric strain reaches high values under the impact zone covered by vegetation, especially for case 1_3 (Fig. 15). However, all the solutions give approximately the same technical outcome, even if the initials conditions of the three vegetated soils are different in terms of initial suction, mechanical and hydrological properties.

It is also significant noticing that pore water pressure dissipation is more efficient in those cases when pore water does not reach so high values. This is because the overall landslide process is very fast, mainly governed by the falling material splashing on the slope beneath and propagating rapidly downslope. In this situation, a key for reduce the inception of a debris avalanche is to keep the pore water pressures as lower as possible in the impact zone (zone 2 of Fig. 4). Doing that, pore water pressures do not increase so much neither below (zone 3 of Fig. 4).

Those numerical analyses were also performed for all the cases of Table 5, including those configurations where the vegetated soils are present over large distances, namely configuration “Geo 1” and “Geo 2” of Table 3, with $B_v = 50$ m and $B_v = 105$ m, respectively. The results are practically similar to those shown until now, despite a more extensive use of vegetated soils.

Table 5 Simulation schemes and range of initial soil suction along the slope

ID	Vegetation species	Installation mode	s_o (kPa)	$s_{o,v}$ (kPa)
0	-	-	5.8–7.8	-
1_1	VEG1	Geo 1	6.4	10.5–12.8
1_2	VEG1	Geo 2	6.3–7.9	7.8–13.4
1_3	VEG1	Geo 3	6.3–7.8	10.4–13
2_1	VEG2	Geo 1	6.4	13.7–19.6
2_2	VEG2	Geo 2	6.8–8	9.2–21
2_3	VEG2	Geo 3	6.3–7.8	13–20
3_1	VEG3	Geo 1	6.2	5.4–5.7
3_2	VEG3	Geo 2	6.2–7.8	5.2–5.8
3_3	VEG3	Geo 3	6.3–7.8	5.3–6.3

s_o suction values within the non-vegetated soil, $s_{o,v}$ suction values within the vegetated soil

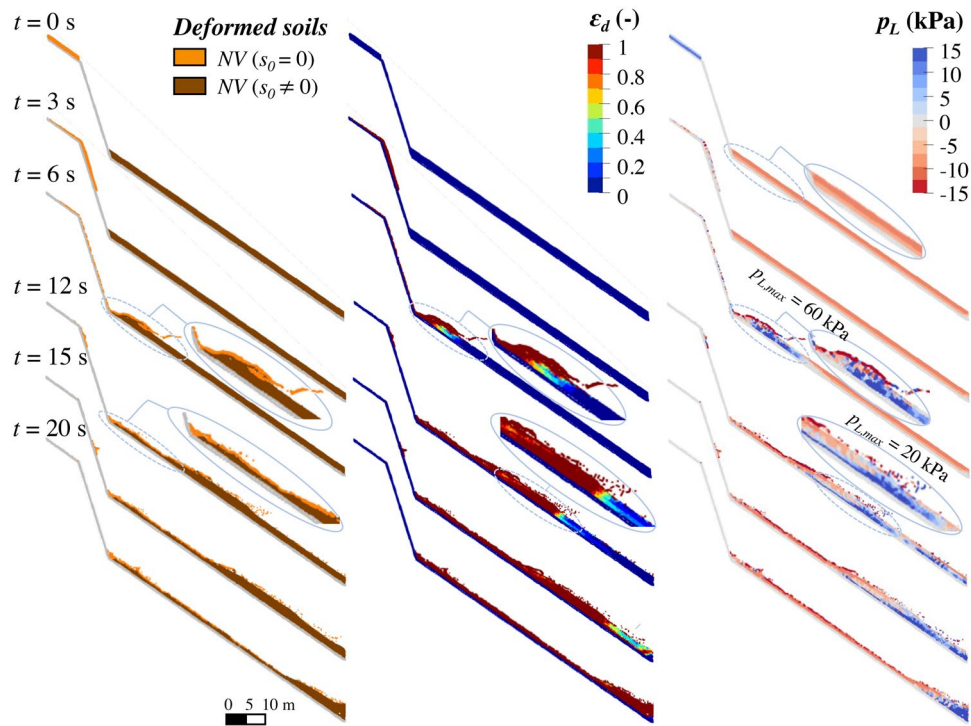


Fig. 14 Spatial distribution of displaced soil, deviatoric strains, and liquid pressure (case 0)

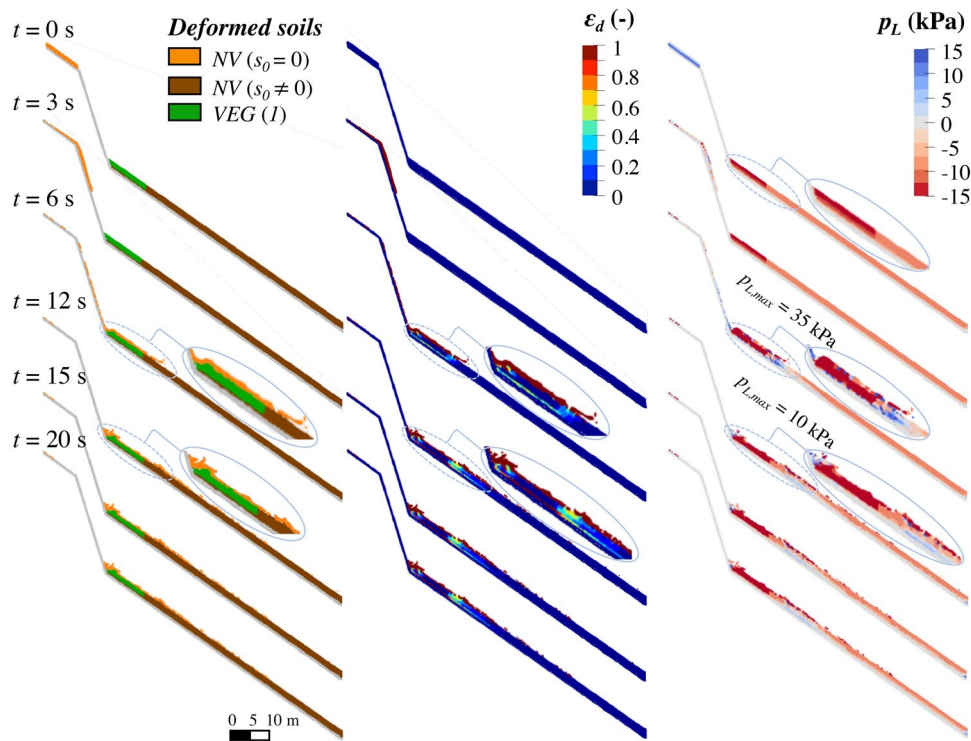


Fig. 15 Spatial distribution of soil, deviatoric strain, and liquid pressure (Case 1_3 with $E = 5$ MPa)

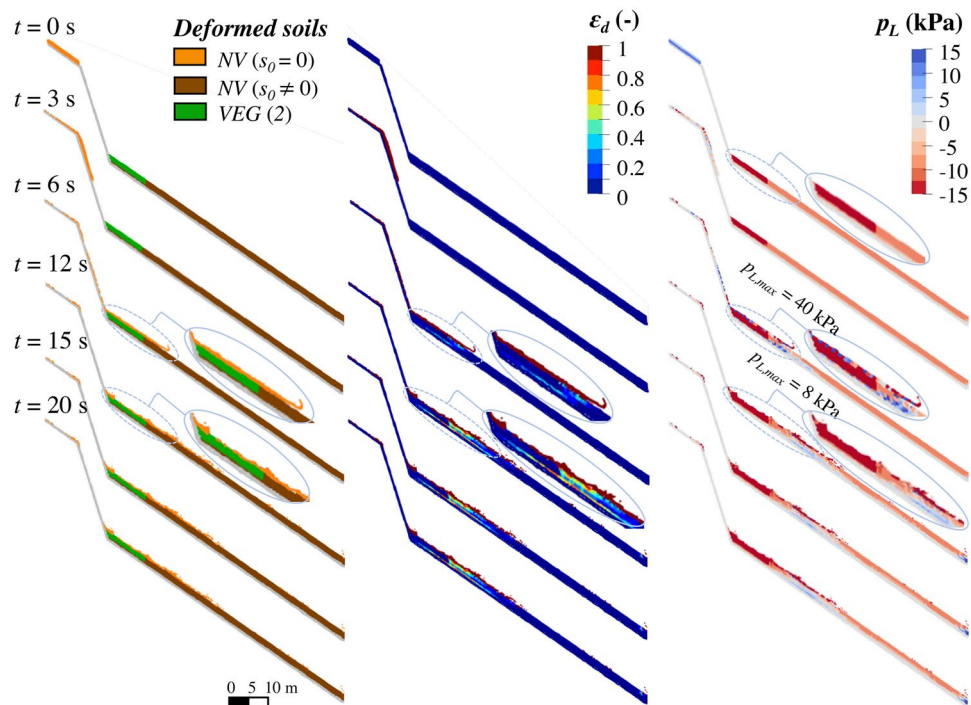


Fig. 16 Spatial distribution of soil, deviatoric strains, and liquid pressure (Case 2_3 with $E=5$ MPa)

Discussion

The numerical results can be explored further to understand the potential of this proposed mitigation technique based on the use of artificially grown long-rooted grasses in specific zones of a slope prone to

the inception of a debris avalanche. For instance, focusing the attention on two material points of the slope initially located inside the so-called zone 2 of Fig. 4 (point A) and zone 3 of Fig. 4 (point B), it is possible to follow their displacements and, in the meantime, track the value of

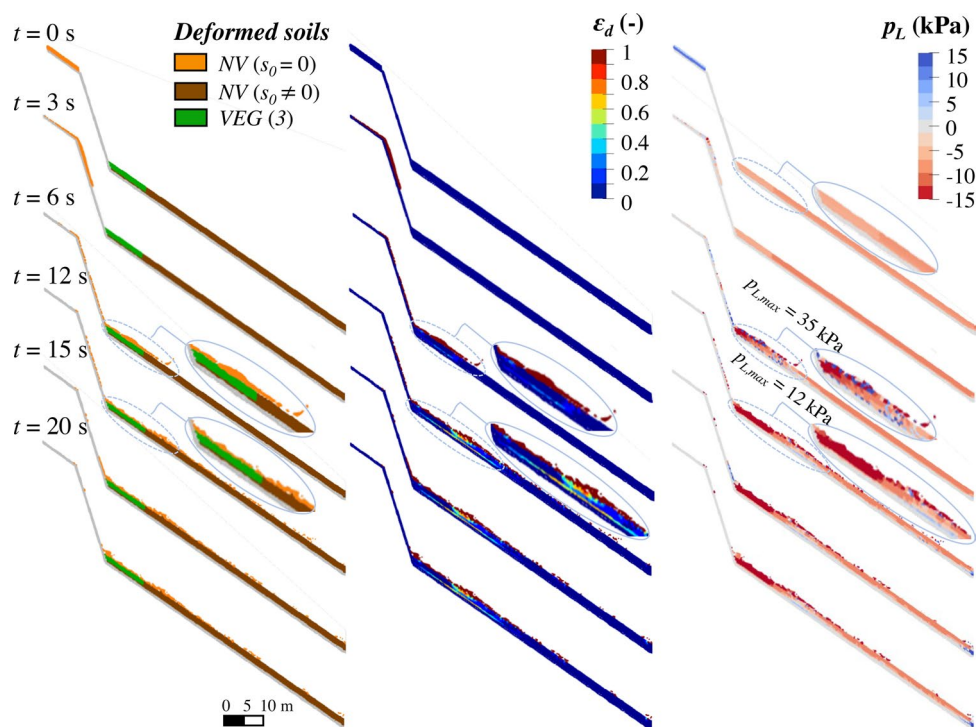


Fig. 17 Spatial distribution of soil, deviatoric strains, and liquid pressure (Case 3_3 with $E=5$ MPa)

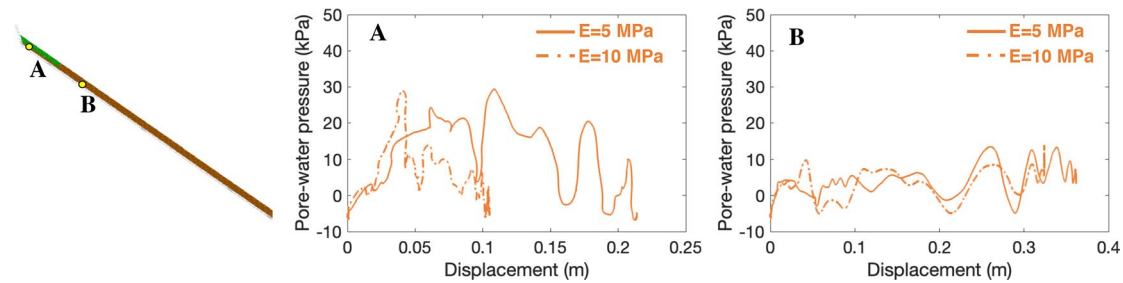


Fig. 18 Evolution of pore water pressure versus displacement for two reference moving points (A and B) for Case 3_3 and two values of stiffness for the rooted soils ($E=5$ MPa, as original soil, and $E=10$ MPa as an effect of root soil improvement)

pore water pressure. These results are shown in Fig. 18. First, it can be observed that the maximum pore water pressures at point A are larger than in point B. This is obviously because point A is in the impact zone. However, it is interesting noting that the point A is displaced less than point B, because the impact zone is reinforced with vegetation (VEG) while point B is in an un-reinforced zone (NV). Then, it is worth of consideration the role played by the stiffness of vegetated soil, equal to the original value or increased as an effect of root soil improvement. No significant difference is found for point B, while some clues can be pointed out for point A. Here, the increased stiffness of the reinforced soil diminishes the maximum displacement to half. The maximum pore water pressure is instead similar than in the other cases, since it is related to the external loading, which is the same (i.e., the falling material). On the contrary, pore water pressure dissipation is much faster for higher stiffness of the reinforced soil. Additional plots and discussion about how the pore water pressures develop with respect to the deviatoric strain are reported in the [Appendix](#).

Conclusions

This paper investigated the use of long-root grass as a possible mitigation technique of debris avalanche. To this aim, three vegetation species were grown in a field test area nearby some slopes affected in the past by catastrophic flow-like landslides such as debris avalanches. The three vegetation species (VEG1, VEG2, VEG3) were seeded in an experimental field, organized into square 9 plots, each $1\text{ m} \times 1\text{ m}$ large. The seeding was done under controlled conditions and the root growth monitored over the months. The rooted soils were later sampled, and geotechnical laboratory soil testing aimed to evaluate the modifications in soil water retention curve and soil shear strength. In the field the variation of soil suction in the rooted soil was also tested.

Such experimental information was implemented in an advanced numerical modelling based on material point method. In this context, the hydro-mechanical coupling between solid skeleton and pore-water is considered from the landslide triggering to the later evolution into a debris avalanche. In particular, the numerical results provided new insights in understanding the complex inception of a debris avalanche, due the impact of a failed soil mass on a stable deposit. The spatio-temporal evolution of stress, strain, and pore-water pressure was computed. The results achieved outline that impact loading can cause further failures in downslope stable deposit. Due to the impact of an unstable mass, a greater volume is mobilized due to the increase in pore-water pressures.

In a modified (engineered) slope condition, the installation of fine long-rooted grasses reduces the effects of the impact loading to a much smaller extent. The reason is that soil is less sheared at the impact zone, and the pore water pressure are less increased than before. Given that, the zone located immediately downslope is less thrust and the overall slope destabilization is practically inhibited. The numerical analyses are not exhaustive neither for the initial soil suction nor for initial unstable mass causing the impact loading scenario and/or the possible slope geometry configurations. Thus, further research is needed to deepen the study of the mechanisms governing the inception and formation of debris avalanches. Nevertheless, the results so far acquired are promising and may pave the way towards the use of vegetation as landslide mitigation technique.

Acknowledgements

The authors would like to acknowledge Prati Armati S.r.l. that provided the grass species used for the tests and eng. Prisco Gambardella for the technical support in the experimental field activities. All MPM simulations were carried out using a version of the Anura3D code (www.anura3D.com) developed in-house by Deltares.

Author contribution

Sabatino Cuomo is responsible for conceptualization, data collection, and numerical modelling. Mariagiovanna Moscariello is responsible for the experimental field and laboratory soil testing. Angela Di Perna is responsible for the data collection, numerical modelling, and the corresponding passages in the manuscript. Mario Martinelli is responsible for numerical modelling and conceptualization. The authors read and approved the final manuscript.

Funding

Open access funding provided by Università degli Studi di Salerno within the CRUI-CARE Agreement. The research was supported by a number of Italian Research Projects funded by the Italian Education and Research Ministry such as Project FARB 2017 “Numerical modelling and inverse analysis for flow-like landslides”; Project FARB 2014 “Large area analysis of triggering and propagation landslide susceptibility for flow-like landslides”; Project FARB 2012 “New Frontiers of advanced numerical simulation of destructive landslides.” This research has been partly supported partly by MIUR PON R&I 2014–2020 Program (project MITIGO, ARSo1_00964).

Availability of data and supporting material

Please contact author for data requests.

Declarations

Competing interests The authors declare no competing interests.

Appendix

The generation of pore water pressure is a key factor for debris avalanche inception. Figure 19 shows the variation of pore water pressure plotted versus the cumulated deviatoric strain (Eq. 6) experienced by the two moving points A and B. The installation of vegetation in the impact zone reduces so much the shearing of soil, as expected, independent on the value of soil stiffness. However, the reduction of deviatoric strain is much more evident in the point B, meaning that the inception of debris avalanche is practically inhibited.

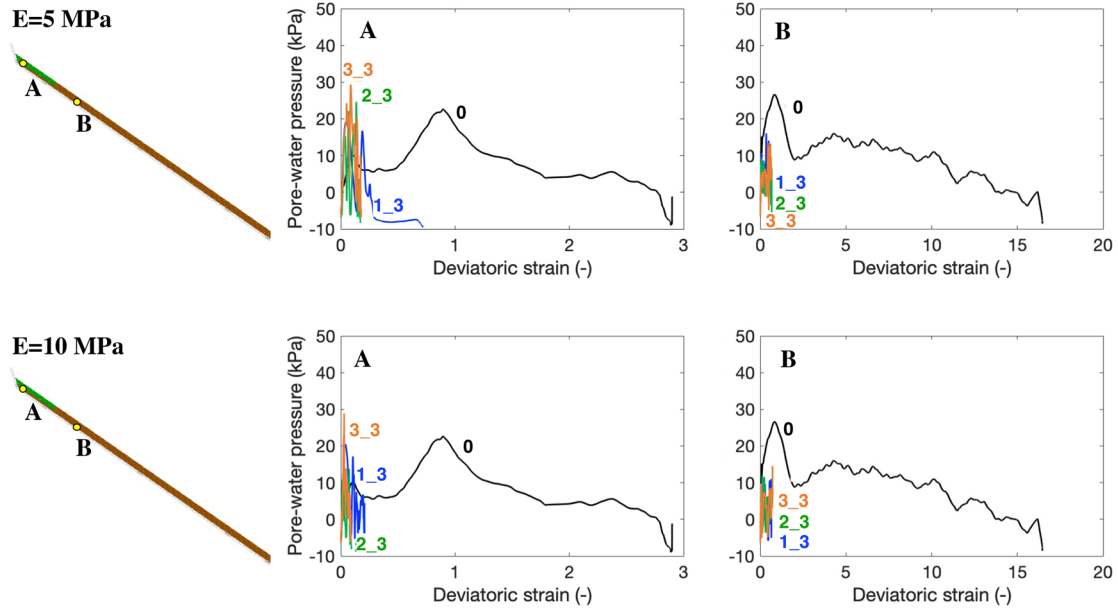


Fig. 19 Generation and dissipation of pore water pressure upon shearing in two reference moving points (A and B) in the natural slope (0) and for different mitigation options (VEG1, VEG2, and VEG3)

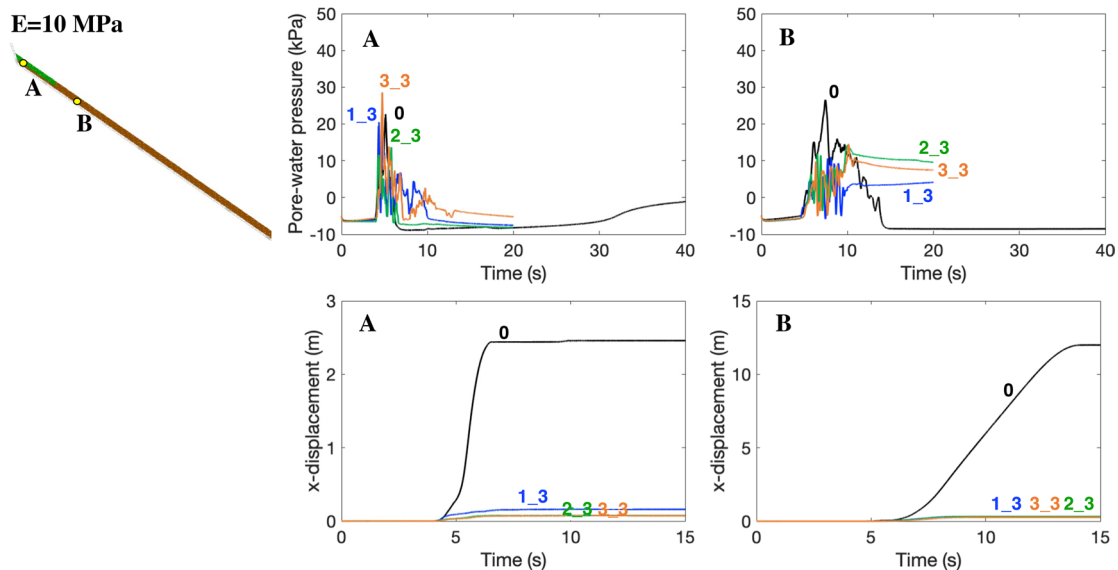


Fig. 20 Temporal trends of pore-water pressure and displacements of two reference moving points (A and B) in the natural slope (0) and for different mitigation options (VEG1, VEG2, and VEG3)

Additional information can be achieved by investigating the trend of pore water pressures and displacements over time inside the impacted zone and within the non-vegetated soil (Fig. 20). The pore-water pressure trend for point A is almost the same in all the cases, with high values at moment of the impact (between 5 and 8 s) and with a plateau in correspondence of the initial suction value right after. However, the displacement of point A is the highest for the case without remediation. Point B is again an interesting point to monitor since there is no vegetated soil above it. Here, some differences are more evident. In fact, for case o, the impact of the unstable mass causes a delayed and more prolonged increase of excess liquid with respect to point A. During this increase in pressures, point B is moving fast and finally reaches a runout of about 12 m.

When the remediation measure is installed, the pore-water pressure is lower than case o, with a maximum of 10 kPa which remains constant over time. The displacement trends for these cases are almost nil, highlighting the efficacy of the proposed solutions. It is worth mentioning that even the other cases in Table 5 with different installation modes are satisfactory.

Open Access This article is licensed under a Creative Commons Attribution 4.0 International License, which permits use, sharing, adaptation, distribution and reproduction in any medium or format, as long as you give appropriate credit to the original author(s) and the source, provide a link to the Creative Commons licence, and indicate if changes were made. The images or other third party material in this article are included in the article's Creative Commons licence, unless indicated otherwise in a credit line to the material. If material is not included in the article's Creative Commons licence and your intended use is not permitted by statutory regulation or exceeds the permitted use, you will need to obtain permission directly from the copyright holder. To view a copy of this licence, visit <http://creativecommons.org/licenses/by/4.0/>.

References

- Bilotta E, Cascini L, Foresta V, Sorbinow G (2005) Geotechnical characterisation of pyroclastic soils involved in huge flowslides. *Geotech Geol Eng* 23:365–402
- Bilotta E, Foresta V, Migliaro G (2008) The influence of suction on stiffness, viscosity and collapse of some volcanic ashy soils. In 1st European conference on unsaturated soils, Durham, England (Vol. 1, pp. 349–354)
- Bishop AW (1954) The use of pore-pressure coefficients in practice. *Geotechnique* 4(4):148–152
- Boldrin D, Leung AK, Bengough AG (2017) Root biomechanical properties during establishment of woody perennials. *Ecol Eng* 109:196–206
- Capobianco V (2018) The effects of roots on the hydro-mechanical behavior of unsaturated pyroclastic soils. PhD Thesis, University of Salerno, Italy
- Capobianco V, Cascini L, Cuomo S, Foresta V (2020) Wetting–drying response of an unsaturated pyroclastic soil vegetated with long-root grass. *Environ Geotech* 40:1–19
- Capra L, Lugo-Hubp J, Borselli L (2003) Mass movements in tropical volcanic terrains: the case of Teziutlán (México). *Eng Geol* 69(3–4):359–379
- Cascini L, Cuomo S, Guida D (2008a) Typical source areas of May 1998 flow-like mass movements in the Campania region, Southern Italy. *Eng Geol* 96:107–125
- Cascini L, Cuomo S, Pastor M, Sorbino G (2010) Modeling of rainfall-induced shallow landslides of the flow-type. *J Geotech Geoenvironmental Eng* 136(1):85–98
- Cascini L, Cuomo S, Pastor M (2013) Inception of debris avalanches: remarks on geomechanical modelling. *Landslides* 10:701–711
- Cascini L, Cuomo S, Pastor M, Fernández-Merodo JA (2008b) Geomechanical modelling of triggering mechanisms for rainfall-induced triangular shallow landslides of the flow-type. Proceedings of the iEMSs Fourth Biennial Meeting: International Congress on Environmental Modelling and Software (iEMSs 2008). 7–10 July 2008, Barcelona, Spain. M. Sánchez-Marré, J. Béjar, J. Comas, A.E. Rizzoli, G. Guariso (eds.). Published by iEMSs, Manno, Switzerland. ISBN: 978-84-7653-074-0, pp. 1516–1523
- Cascini L, Sorbino G, Cuomo S, Ferlisi S (2014) Seasonal effects of rainfall on the shallow pyroclastic deposits of the Campania region (southern Italy). *Landslides* 11:779–792
- Ceccato F, Yerro A, Martinelli M (2018) Modelling soil-water interaction with the material point method. Evaluation of single-point and double-point formulations. In *Numerical methods in geotechnical engineering IX* (pp. 351–358). CRC Press
- Chen H, Crosta GB, Lee CF (2006) Erosional effects on runout of fast landslides, debris flows and avalanches: a numerical investigation. *Geotechnique* 56(5):305–322
- Costa JE, Williams GP (1984). Debris-flow dynamics (No. 84-606). U.S. Geological Survey. Open-File Report
- Cuomo S (2014) New advances and challenges for numerical modeling of landslides of the flow type. *Procedia Earth Planet Sci* 9:91–100. <https://doi.org/10.1016/j.proeps.2014.06.004>
- Cuomo S (2020) Modelling of flowslides and debris avalanches in natural and engineered slopes: a review. *Geoenvironmental Disasters* 7:1–25
- Cuomo S, Di Perna A, Martinelli M (2021b) Modelling the spatio-temporal evolution of a rainfall-induced retrogressive landslide in an unsaturated slope. *Eng Geol* 294:106371
- Cuomo S, Moscariello M, Foresta V (2017) Wetting tests of partially saturated soils under simple shear conditions. *Geotech Lett* 7(2):197–203
- Cuomo S, Pastor M, Cascini L, Castorino GC (2014) Interplay of rheology and entrainment in debris avalanches: a numerical study. *Can Geotech J* 51(11):1318–1330
- Cuomo S, Pastor M, Capobianco V, Cascini L (2016) Modelling the space-time evolution of bed entrainment for flow-like landslides. *Eng Geol* 212:10–20
- Cuomo S, Prime N, Iannone A, Dufour F, Cascini L, Darve F (2013) Large deformation FEM-LIP drained analysis of a vertical cut. *Acta Geotech* 8:125–136
- Cuomo S, Foresta V, Moscariello M (2015) Shear strength of a pyroclastic soil measured in different testing devices. *Volcanic Rocks and Soils* 137
- Cuomo S, Di Perna A, Martinelli M (2021a) Inception of debris avalanches: a material point method modelling. In *Advanced Tunneling Techniques and Information Modeling of Underground Infrastructure: Proceedings of the 6th GeoChina International Conference on Civil & Transportation Infrastructures: From Engineering to Smart & Green Life Cycle Solutions--Nanchang, China, 2021 6* (pp. 1–15). Springer International Publishing
- Ehleringer JR, Cerling TE (2002) C3 and C4 photosynthesis. *Encyclopedia of Global Environmental Change* 2(4):186–190
- Ekanayake JC, Phillips CJ (2002) Slope stability thresholds for vegetated hillslopes: a composite model. *Can Geotech J* 39(4):849–862
- Fan CC, Su CF (2008) Role of roots in the shear strength of root-reinforced soils with high moisture content. *Ecol Eng* 33(2):157–166
- Foresta V, Capobianco V, Cascini L (2020) Influence of grass roots on shear strength of pyroclastic soils. *Can Geotech J* 57(9):1320–1334
- Fratiani F, Cardinale F, Cozzolino A, Granese T, Albanese D, Di Matteo M, Zaccardelli M, Coppola R, Nazzaro F (2014) Polyphenol composition and antioxidant activity of different grass pea (*Lathyrus sativus*), lentils (*Lens culinaris*), and chickpea (*Cicer arietinum*) ecotypes of the Campania region (Southern Italy). *J Funct Foods* 7:551–557

- Fredlund DG, Rahardjo H (1993) Soil mechanics for unsaturated soils. John Wiley & Sons
- Fuchu D, Lee CF, Sijing W (1999) Analysis of rainstorm-induced slide-debris flows on natural terrain of Lantau Island, Hong Kong. *Eng Geol* 51(4):279–290
- Guadagno FM, Revellino P (2005) Debris avalanches and debris flows of the Campania Region (southern Italy). In Jakob, M., Hungr, O. (Eds.), *Debris-flow Hazard and Related Phenomena*. Springer, 489–518
- Hargreaves GH (1975) Moisture availability and crop production. *Transactions of the ASAE* 18(5):980–0984
- Hughes TJ (2012) The finite element method: linear static and dynamic finite element analysis. Courier Corporation
- Hungr O, Evans S, Bovis MJ, Hutchinson JN (2001) Landslides of the Flow Type. *Environ Eng Geosci* 7(3):221–238
- Hungr O, McDougall S, Wise M, Cullen M (2008) Magnitude–frequency relationships of debris flows and debris avalanches in relation to slope relief. *Geomorphology* 96(3–4):355–365
- Hutchinson JN, Bhandari RK (1971) Undrained loading, a fundamental mechanism of mudflow and other mass movements. *Geotechnique* 21(4):353–358
- Jassim I, Stolle D, Vermeer P (2013) Two-phase dynamic analysis by material point method. *Int J Numer Anal Meth Geomech* 37(15):2502–2522
- Lacerda WA (2004) The behavior of colluvial slopes in a tropical environment. In *Landslides: evaluation and stabilization* (pp. 1315–1342)
- Leung AK, Garg A, Ng CWW (2015) Effects of plant roots on soil-water retention and induced suction in vegetated soil. *Eng Geol* 193:183–197
- Leung AK, Kamchoom V, Ng CWW (2017) Influences of root-induced soil suction and root geometry on slope stability: a centrifuge study. *Can Geotech J* 54(3):291–303
- Martinelli M, Lee WL, Shieh CL, Cuomo S (2021) Rainfall boundary condition in a multiphase Material Point Method. *Understanding and Reducing Landslide Disaster Risk: Volume 4 Testing, Modeling and Risk Assessment 5th*, 303–309
- Martinelli M, Galavi V (2022) An explicit coupled MPM formulation to simulate penetration problems in soils using quadrilateral elements. *Comput Geotech* 145:104697
- Mendicino G, Senatore A (2013) Regionalization of the Hargreaves coefficient for the assessment of distributed reference evapotranspiration in Southern Italy. *J Irrig Drain Eng* 139(5):349–362
- Mickovski SB, Hallett PD, Bransby MF, Davies MC, Sonnenberg R, Bengough AG (2009) Mechanical reinforcement of soil by willow roots: impacts of root properties and root failure mechanism. *Soil Sci Soc Am J* 73(4):1276–1285
- Monteith JL (1965) Evaporation and environment. In *Symposia of the society for experimental biology* (Vol. 19, pp. 205–234). Cambridge University Press (CUP) Cambridge
- Moscariello M, Chen Y, Cuomo S, Buscarnera G (2020) Modelling of simple shear tests on volcanic unsaturated sands. In *E3S web of conferences* (Vol. 195, p. 02021). EDP Sciences
- Moscariello M, Cuomo S, Baumann V, Bonadonna C (2021) On the features of pyroclastic deposits and post-eruption natural hazards. In *Geohazard Mitigation: Select Proceedings of VCDRR 2021* (pp. 157–170). Singapore: Springer Singapore
- Ng C, Leung A, Kamchoom V, Garg A (2014) A novel root system for simulating transpiration-induced soil suction in centrifuge. *Geotech Test J* 37(5):733–747
- Ng CWW, Garg A, Leung AK, Hau BCH (2016a) Relationships between leaf and root area indices and soil suction induced during drying–wetting cycles. *Ecol Eng* 91:113–118
- Ng CWW, Kamchoom V, Leung AK (2016b) Centrifuge modelling of the effects of root geometry on transpiration-induced suction and stability of vegetated slopes. *Landslides* 13:925–938
- Ng CWW, Leung AK, Woon KX (2013a) Effects of soil density on grass-induced suction distributions in compacted soil subjected to rainfall. *Can Geotech J* 51(3):311–321
- Ng CWW, Ni JJ, Leung AK, Wang ZJ (2016c) A new and simple water retention model for root-permeated soils. *Geotech Lett* 6(1):106–111
- Ng CWW, Woon KX, Leung AK, Chu LM (2013b) Experimental investigation of induced suction distribution in a grass-covered soil. *Ecol Eng* 52:219–223
- Ni JJ, Leung AK, Ng CWW (2017) Investigation of plant growth and transpiration-induced matric suction under mixed grass-tree conditions. *Can Geotech J* 54(4):561–573. <https://doi.org/10.1139/cgj-2016-0226>
- Preti F, Schwarz M (2006) On root reinforcement modelling. *Geophysical Research* 436 Abstracts, vol. 8, EGU General Assembly. ISSN: 1029-7006
- Sassa K, Fukuoka H, Wang F (1997) Gamahara torrent debris flow on 6 December 1996, Japan: Possible mechanism of the debris flow. *Landslide News* 10:6–9
- Sassa K, Wang G, Fukuoka H (2003) Performing undrained shear tests on saturated sands in a new intelligent type of ring shear apparatus. *Geotech Test J* 26(3):257–265
- Soga K, Alonso E, Yerro A, Kumar K, Bandara S (2016) Trends in large-deformation analysis of landslide mass movements with particular emphasis on the material point method. *Géotechnique* 66(3):248–273
- Stokes A, Atger C, Bengough AG, Fourcaud T, Sidle RC (2009) Desirable plant root traits for protecting natural and engineered slopes against landslides. *Plant Soil* 324:1–30
- Strumia S, Buonanno M, Aronne G, Santo A, Santangelo A (2020) Monitoring of plant species and communities on coastal cliffs: Is the use of unmanned aerial vehicles suitable? *Diversity* 12(4):149
- Sulsky D, Chen Z, Schreyer HL (1994) A particle method for history-dependent materials. *Comput Methods Appl Mech Eng* 118(1–2):179–196
- Switala BM (2016) Analysis of slope stabilization by soil bioengineering methods analysis of slope stabilisation by soil bioengineering methods. University of Natural Resources and Life Sciences
- Szarek SR, Ting IP (1975) Photosynthetic Efficiency of CAM Plants in Relation to C3 and C4 Plants. In Marcelle, R. (eds) *Environmental and biological control of photosynthesis*. Springer, Dordrecht. https://doi.org/10.1007/978-94-010-1957-6_29
- Tagarelli V (2019) Analysis of the slope-vegetation-atmosphere interaction for the design of the mitigation measures of landslide risk in clayey slopes (Doctoral dissertation, Politecnico di Bari)
- Take WA, Bolton MD, Wong PCP, Yeung FJ (2004) Evaluation of landslide triggering mechanisms in model fill slopes. *Landslides* 1:173–184
- Van Genuchten MT (1980) A closed-form equation for predicting the hydraulic conductivity of unsaturated soils. *Soil Sei Am J* 44:892–989
- Wang FW, Sassa K, Fukuoka H (2003) Downslope volume enlargement of a debris slide-debris flow in the 1999 Hiroshima, Japan, rainstorm. *Eng Geol* 69:309–330
- Wang FW, Sassa K, Wang G (2002) Mechanism of a long-runout landslide triggered by the August 1998 heavy rainfall in Fukushima Prefecture, Japan. *Eng Geol* 63(1–2):169–185
- Wu TH (2013) Root reinforcement of soil: Review of analytical models, test results, and applications to design. *Can Geotech J* 2013(50):259–274
- Wu TH, McKinnell WP III, Swanston DN (1979) Strength of tree roots and landslides on Prince of Wales Island, Alaska. *Can Geotech J* 16(1):19–33
- Yerro A, Girardi V, Martinelli M, Ceccato F (2022) Modelling unsaturated soils with the Material Point Method. A discussion of the state-of-the-art. *Geomech Energy Environ* 32:100343
- Yildiz A, Graf F, Rickli C, Springman SM (2018) Determination of the shearing behaviour of root-permeated soils with a large-scale direct shear apparatus. *CATENA* 166:98–113

Sabatino Cuomo (✉) · **Angela Di Perna** ·

Mariagiovanna Moscariello

Geotechnical Engineering Group (GEG), University of Salerno, Via Giovanni Paolo II, 132, 84084 Fisciano, (SA), Italy
Email: scuomo@unisa.it

Mario Martinelli

GEO Unit, DELTARES, Boussinesqweg, 1, 12629 HV Delft, Netherlands
Email: mario.martinelli@deltares.nl

Mario Martinelli

Adjunct Research Professor, Department of Civil and Environmental
Engineering, Carleton University, 1125 Colonel By Dr, On K1S 5B6,
Ottawa, Canada
Email: mario.martinelli@deltares.nl